Supporting Information

Sinai et al. 10.1073/pnas.0913422107

Additional Features of NK Cell Polarization: IL-15 NK Cells, MTOC Reorientation, and Delivery of the Lytic Hit

In addition to characterizing the polarization of NK cells primed with IL-12/18, we addressed priming with another innate cytokine, IL-15. Actin accumulation in the interaction of IL-15 NK cells with YAC-1 target cells was moderate and transient, similar to IL-12/18 NK cells. Only 1.5 ± 0.3% of actin was moved to the interface at the time of tight cell couple formation (Fig. 1*A*). This accumulation was essentially stable, with a modest decline 5 to 7 min after tight cell coupling that did not reach significance (Fig. 1*A* and Fig. S2*A*). However, in lytic interactions the average amount of actin moved to the interface decreased rapidly from 2.5 ± 0.7% at the time of tight cell coupling to 0.5% to 1.0% thereafter, establishing transience (Fig. S2*C*). In contrast, the average amount of actin moved to the interface remained above 1.5% in nonkilling interactions (Fig. S2*C*). IL-15 NK cells thus displayed the same relation between transient polarization and target cell lysis as IL-12/18 NK cells (Fig. 1*B*).

Corroborating substantial differences in the polarization of IL-12/18 and IL-2 NK cells, delivery of the lytic hit and MTOC reorientation were also distinct. Delivery of the lytic hit by IL-2 NK cells triggered mostly blebbing (Movie S1, Movie S2, and Movie S3), similar to CTLs (1). In contrast, delivery of the lytic hit by IL-12/18 and IL-15 NK cells resulted in dramatic target cell damage, allowing unambiguous distinction between lytic and nonkilling interactions (Movie S4, Movie S5, Movie S6, and Movie S7). Indicative of decisive polarization of IL-2 NK cells, 88 ± 8% of IL-2 NK cells reoriented the MTOC toward the interface within 2 min of tight cell couple formation (Fig. S2*F* and Movie S8), comparable to CTLs (96 ± 4%) but much more rapidly than IL-12/18 NK cells (90% of nonkilling interactions do not reorient the MTOC at all) (1).

In summary, analyzing interface actin dynamics (main text and here), MTOC reorientation, and delivery of the lytic hit together establish that priming the same B6 splenocytes with innate cytokines versus IL-2 generates NK cells with fundamentally different polarization behavior. Importantly, polarization of human ex vivo NK cells (2, 3) resembles that of murine NK cells primed with innate cytokines but not with IL-2.

Cdc42 Is the Dominantly Expressed Rho GTPase in NK Cells

As determined by real-time PCR (Fig. S3*A*), mRNA for Cdc42 was approximately five times as abundant as that of Rac1, the plasma membrane–associated Rac isoform, in all NK cells. mRNA levels of Rac2, the isoform predominantly associated with internal membranes (4), were only moderately lower than those of Cdc42. Cdc42 expression relative to MHC I was virtually identical in IL-2 and IL-12/18 NK cells (Fig. S3*A*).

Accumulation of Active Cdc42 at the Lymphocyte/Target Cell Interface Is Less Intense Yet More Central in CTLs than in Helper T Cells and NK Cells

The features of interface accumulation of active Cdc42 resembled those of actin across all cytolytic effectors (Table S1). This similarity implicates Cdc42 as a critical actin regulator, as corroborated by direct interference with Cdc42 activation. In particular, transience and its relation to cytolysis were fully matched. Interestingly, IL-12/18 NK cells combined intermediate interface Cdc42 activity with modest actin accumulation, whereas CTLs turned limited Cdc42 activity into intense interface actin accumulation (Figs. 1*A* and 3*A*). We suggest that focusing Cdc42 activity on the center of the interface allowed CTLs to generate intense actin accumulation with more limited amounts of active Cdc42, as supported by data from helper T cells (5). Other explanations, such as comparably higher interface Rac activity in CTLs (as detailed later) are certainly possible.

Interface accumulation of active Cdc42 was also more than fivefold lower in P14 CTLs than in the activation of various helper T cells under comparably strong activation conditions (Fig. S3*E*) (6). Complete cessation of interface accumulation of active Cdc42 was not observed in helper T cells. Weaker and more transient interface accumulation in P14 CTLs extended to other signaling intermediates, e.g., linker for activation of T cells (LAT; Fig. S3*F*). These data are consistent with the need for more transient cellular interactions in CTLs to allow effective sequential target cell killing.

Less Intense Polarization Was Related to Reduced Target Cell Killing When Strong and Weak Stimuli Were Compared in IL-12/18 NK Cell/Target Cell Interactions

To assert that effective cytolytic effector polarization remains related to effective target cell lysis upon large differences in the extent of polarization, we studied the interaction of IL-12/18 NK cells and P815 target cells incubated with anti-NKG2D. P815 cells are inherently resistant targets. Incubation with anti-NKG2D allows limited NK cell activation through redirected engagement of only one activating receptor, NKG2D. NK cell polarization under these conditions was inefficient. No more than 0.45 ± 0.2% of actin was moved to the interface at any time (Fig. 1*A*). Transience of actin accumulation was almost entirely lost, as accumulation at 7 min after cell coupling was virtually identical to that at cell coupling (Fig. 1*A* and Fig. S2*B*). Similarly, accumulation of active Cdc42 at the interface did not increase to more than 0.6 ± 0.1% of the sensor for active Cdc42 moved to the interface (Fig. 3*A*), significantly less than IL-12/18 NK cells activated by YAC-1 targets [$P < 0.001$ at all time points but the last ($P < 0.05$)]. Interface accumulation of active Cdc42 was still transient in lytic cell couples, with significantly more sensor accumulation ($P < 0.05$) detectable at cell coupling (1.1 ± 0.2% of sensor for active Cdc42 moved to the interface) than 5 min thereafter (0.05%–0.4%; Fig. S3*D*). Confirming that dramatically reduced polarization was related to low killing activity, specific target cell lysis at 13 ± 2.5% (20: 1 effector-to-target cell ratio) was significantly lower ($P < 0.02$) than that of all other effector/target cell conditions tested (Fig. 1*C*). This was most likely caused by a significant ($P < 0.001$) decrease in the percentage of NK cells forming tight cell couples upon target cell contact from 72 ± 4% in response to YAC-1 targets to 22 ± 4% in response to P815/anti-NKG2D (Fig. S5*D*). Once formed, a comparable percentage of cell couples progressed to target cell lysis (30.5% vs. 33.5%; Fig. S5*D*). In summary in the activation of IL-12/18 NK cells, a weaker stimulus affected cell couple formation and the amount of actin and active Cdc42 recruited to the NK cell/target cell interface. These changes are consistent with impaired target cell lysis. However, the selective transience of the accumulation of active Cdc42 in lytic versus nonkilling interactions and the ability of a tight cell couple to progress to target cell lysis were preserved, suggesting conservation of the role of transience in facilitating target cell lysis.

Accumulation of Active Rac at the NK Cell/Target Cell Interface Differs from That of Active Cdc42

In comparison with active Cdc42, accumulation of active Rac at the NK cell/target cell interface (Figs. S3 *G–I* and S4) was less

intense. Translocation of the Rac sensor to the interface did not exceed 1% for IL-2 and IL-12/18 NK cells (Fig. S3*G*) at all but one time point after tight cell couple formation, whereas Cdc42 sensor translocation was greater than 1% at all but one time point (Fig. 3*A*). In contrast to the accumulation of active Cdc42, accumulation of active Rac was well sustained in both NK cell types (Fig. S3 *G–I*), actually increasing over time. This lack of transience in Rac accumulation supports a selective role of Cdc42 in the regulation of the transience of NK cell polarization. An even balance among central, diffuse, and asymmetric/peripheral patterns in the patterning of active Rac was shared with active Cdc42 (Fig. S3*J*).

In contrast to the divergent intensity and transience of the accumulation of active Rac and Cdc42 in NK cells, accumulation of active Rac at the P14 CTL/EL4 target cell interface (Fig. S3*G* and S4*A*) was comparable to that of Cdc42. It was of moderate intensity with percent sensor translocation to the interface at and after tight cell coupling ranging from 0.2% to 0.6% for Cdc42 and from 0.05% to 1.1% for Rac. Accumulation of active Rac was highly transient; at least 2 min after tight cell coupling the percentage of sensor moved to the interface decreased to less than one tenth of the amount at cell coupling ($P \leq 0.001$ relative to the time of tight cell coupling; Fig. S3 *G* and *H*). Accumulation of active Rac was predominantly central; in 62 ± 5% of time points with accumulation of active Rac this accumulation occurred in the central pattern (Fig. S3*J*).

The selective differences between Rac and Cdc42 in NK cell activation are consistent with at least partially divergent roles of Cdc42dn and Rac1dn in NK cell function. A likely contribution to the more limited Rac activity is the weaker expression of plasma membrane–associated Rac isoform Rac1 versus Cdc42 (Fig. S3*A*). A rigorous investigation of the functional consequences of such weaker Rac activity is beyond the scope of this manuscript. Also understanding why features of the activation of Rac and Cdc42 in CTLs are more similar to each other than observed in NK cells cannot be addressed here.

Rac Is a Critical Regulator of Interface Actin Accumulation/ Rac1dn but Not Cdc42dn Can Interfere with Tight Cell Coupling

Rac1dn (100 nM) consistently reduced interface actin accumulation in all NK cell/target cell interactions (Fig. S5 *A–C*). In contrast to 100 nM Cdc42 (Fig. 4*A*), such reduction extended to lytic interactions of IL12/18 NK cells with YAC-1 target cell. In such interactions, percentage of actin moved to the interface was reduced from 0.5% to 2.3% to no greater than 0.2% at all time points at and after tight cell coupling ($P < 0.001$) upon treatment with 100 nM Rac1dn. Various reasons are conceivable for the more potent effect of 100 nM Rac1. The expression of guanine nucleotide exchange factors for Rac1, the molecular targets of Rac1dn, could be lower than that of Cdc42 guanine nucleotide exchange factors, resulting in more extensive blockade upon application of the same concentration of blocking reagent. This suggestion is consistent with the more limited accumulation of active Rac at the NK cell/target cell interface. Alternatively, the role of Rac in the regulation of actin dynamics could be more general, leaving a more specific role of Cdc42 in nonkilling interactions.

In the interaction of P14 CTLs with EL4 target cells in the presence of 10 μM gp33 agonist peptide, 100 nM Rac1dn yielded transient interference with interface actin accumulation. At time points 1 to 3 min after cell coupling, actin interface accumulation was significantly ($P < 0.01$) reduced (Fig. S5*C*). However, at 7 min no significant difference remained to buffer only. This is in contrast to the effect of 100 nM Cdc42dn, in which suppression of interface actin accumulation was sustained (Fig. S5*C*). The limitation of the suppressive effect of Rac1dn on interface actin accumulation to 1 to 3 min after tight cell couple formation is consistent with the restriction of substantial interface Rac activity to within the first minute after tight cell coupling (Fig. S3 *G* and *H*). The more sustained effect of Cdc42dn is matched by more sustained interface Cdc42 activity at 2 to 5 min, but not 7 min (Fig. 3*A*).

In summary, the effects of Rac1dn and Cdc42dn on cytolytic effector actin dynamics differed frequently, establishing specificity. Moreover, spatiotemporal features of actin regulation by Rac1dn and Cdc42dn matched patterns of interface accumulation of the active GTPases, supporting spatiotemporally constrained roles of Rac and Cdc42 in cytolytic effector activation.

The ability to rapidly recruit actin to the effector/target cell interface is critical for the formation of tight cell couples. Cdc42dn (100 nM) did not interfere with cell coupling in any of the interactions of cytolytic effectors with susceptible targets (Fig. S5 *D–F*) Similar to 100 nM Cdc42, cell coupling of P14 CTLs and IL-2 NK cells was also undisturbed by treatment with 100 nM Rac1dn (Fig. S5 *E* and *F*). However, 100 nM Rac1dn reduced the percentage of IL-12/18 NK cells that form a tight cell couple upon contact with YAC-1 target cells significantly ($P < 0.001$) from 72 ± 3.5% upon treatment with buffer only to 20.5 ± 4% (Fig. S5*D*). The greater sensitivity of IL-12/18 NK cells to 100 nM Rac1dn is consistent with the lower intensity of interface actin accumulation in IL-12/18 NK cells as compared with CTLs and IL-2 NK cells. Rac1dn (100 nM) further reduces it (Fig. S5*A*), likely below a threshold required for sufficient actin accumulation upon target cell contact. The divergent effects of Cdc42dn and Rac1dn on cell coupling further support the specificity of the two reagents.

The data of this paragraph together with those on Cdc42 in the main text strongly suggest that 100 nM Cdc42dn exerts its dominant effect on actin dynamics in NK cell couple maintenance rather than formation, whereas 100 nM Rac1dn leads to more general interference with actin dynamics. Roles in CTLs differed.

Rac1dn Does Not Enhance the Response Frequency of Cytolytic Effectors in Target Cell Lysis

Cdc42dn consistently enhanced the frequency of cytolytic responders, likely through selective destabilization of nonproductive NK cell/target cell interactions (Fig. 4). Rac1dn did not, establishing specificity for the effect of Cdc42dn: treatment of IL-12/18 NK cells with Rac1dn led to a reduction in bulk YAC-1 target cell killing by 13.5 ± 3.5% ($P = 0.01$; Fig. 4*D*), suggesting that Rac1 activity is required for effective target cell lysis, as previously reported (7). In accordance, CD107a surface expression in response to YAC-1 target cell contact was slightly decreased by 4 ± 1.5% ($P < 0.05$) in IL-12/18 NK cells upon treatment with Rac1dn (Fig. 4*B*). The requirement of Rac for cell coupling (Fig. S5*D*) offers a straightforward explanation why Rac could be required for effective killing. Effects of Rac1dn on IFN-γ secretion were modest at best (Fig. S7).

Cdc42 and Rac thus displayed moderately divergent roles in cytolytic effector function. Their roles can be understood when the differences in the effects of 100 nM Cdc42dn and Rac1dn on interface actin are taken into account: (*i*) in IL-12/18 NK cell/target cell couples Rac1dn virtually eliminated interface actin accumulation (Fig. S5*A*), the strongest effect on actin accumulation seen with any Rho family GTPase in any cytolytic effector. Accordingly, only 100 nM Rac1dn could reduce cell coupling and cytolysis and only in IL-12/18 NK cells. (*ii*) In IL-2 NK cells, where interface actin was strongest and most sustained, even treatment with 100 nM Rac1dn still left modest interface actin (Fig. S5*B*), likely sufficient for effective initial polarization in the regulation of cell coupling and degranulation. Thus, enhancement of effector function by destabilization of nonproductive effector/target cell couples, as widely seen upon treatment with 100 nM Cdc42dn, could come into play under these conditions. In support, the responder frequency in IFN-γ secretion by

IL-2 NK cells was enhanced upon treatment with 100 nM Rac1dn (Fig. S7*A*).

The effects of 100 nM Rac1dn thus reiterate the principal themes in the role of cytolytic effector polarization in effector function found with Cdc42. Minimal polarization was required for function: the most dramatic interference with polarization in response to susceptible targets seen in our studies, 100 nM Rac1dn in IL-12/18 NK cells, yielded impaired target cell lysis. However, once minimal polarization was achieved, spatiotemporal features of polarization, particularly its transience, became dominant: increasing transience in IL-2 NK cells/YAC-1 target cell interactions by suppressing interface actin through treatment with 100 nM Rac1dn enhanced responder frequency in IFN-γ secretion, similar to the Cdc42dn data.

SI Materials and Methods

Imaging. Actin-GFP, tubulin-GFP, and sensors for active Cdc42 and Rac are established (6). The fluorescent proteins were expressed in the cytolytic effectors by retroviral transduction with Moloney murine leukemia virus–based vectors as established (1). Expression levels in the cytolytic effectors were adjusted to a fivefold range at the high end of microscope sensitivity corresponding to 5 μM (6) to minimize interference with cytolytic effector activation (6). Live cell imaging of the interaction of transduced cytolytic effectors and targets (1), cell couple identification (1), and classification of the intensity (5) and patterns (6) of sensor accumulation are established.

Specifically, cytolytic effector/target cell interactions in the presence of 10% FBS were imaged at 37 °C with a ×40, 1.3 NA oil objective or a ×20, 0.75 NA air objective using an imaging system built on the Nikon TE2000-S platform. Acquisition frequencies are indicated in the captions to Movie S1, Movie S2, Movie S3, Movie S4, Movie S5, Movie S6, Movie S7, Movie S8, Movie S9, Movie S10, Movie S11, Movie S12, Movie S13, Movie S14, and Movie S15. One differential interference contrast and 21 fluorescence images were acquired. The 21 fluorescence images spanned 20 μm in the z-plane at 1-μm intervals. A piezoelectric z-motor was used for rapid adjustments along the z-plane. A MicroMax cooled CCD camera (Princeton Instruments) with a 1,300 × 1,030 chip size and a pixel size of 6.7 × 6.7 μm was used without or at 2 × 2 binning with an acquisition time of 200 ms to acquire the images. All 21 images of one z stack were streamed into computer memory for the fastest camera readout. Thus, a single z stack was acquired in 7 s. Imaging system control and image analysis were executed using the Metamorph (Molecular Devices) software package.

Cell coupling was determined in the differential interference contrast images only, without regard for the fluorescence information. The formation of a tight cell couple, time 0 in our analysis, was defined as either the first time point with a fully spread T cell–APC interface or 1 min after first membrane contact, whichever occurred first. Therefore, small initial membrane contact between cytolytic effector and target cell often occurred before time 0 and occasional accumulation of actin and active Cdc42/Rac at the small initial interface could be observed.

The analysis of the intensity of sensor (actin-GFP or sensors for active Cdc42, Rac) accumulation at the cytolytic effector/target cell interface takes into account that average sensor interface accumulation at the population level is driven by two components, the percentage of cytolytic effectors that show interface accumulation above a threshold (140% of cellular background fluorescence) and the amount of cellular actin or signaling sensor that is moved to the effector/target cell interface in the portion of the population that does shown accumulation. As a single measure for interface accumulation at the population level used throughout the manuscript, we therefore multiply the percentage of cell couples with interface accumulation by the average amount of actin or the signaling sensor relative to the total cellular amount that is translocated to the interface as determined for all individual cell couples with sensor accumulation above threshold: the Sensor translocated to the interface (in percent) is equal to the fraction of cell couples above threshold multiplied by the average amount of sensor translocated to the interface.

The percentage of sensor translocated to the interface was determined in 1-min intervals between time points −1 and 10 relative to tight cell couple formation. At later time points, the number of cytolytic effectors with interface sensor accumulation above the 140% intensity threshold was often low (<5). In that case, rolling averages of three time points, e.g., the average of time points 4, 5, and 6 for time point 5, were displayed in the figures as indicated in the figure legends to allow meaningful analysis. To allow an assessment of the two individual components of the percentage of sensor translocated to the interface, the fraction of cell couples above threshold is given separately for key data in Figs. S2*B* and S3 *A* and *I*.

Patterns of accumulation of sensors at the interface were determined with the Metamorph software package. Data used for this analysis were a maximum projection for the identification of the x and y coordinates of an area of accumulation and maximum-type 3D reconstructions or the raw 3D stacks for the determination of the z coordinates. A region of accumulation of a given sensor was defined as a region with an average fluorescence intensity of greater than 140% of the background cellular fluorescence. A time point was scored as "no accumulation" if the fluorescence intensity within a distinct area of interface accumulation was lower than 140% of the background intensity of cellular fluorescence. To classify the spatial features of a bona fide area of accumulation, five mutually exclusive interface patterns were used: central, invagination, diffuse, lamellal, and asymmetric/peripheral, as defined by strict geometrical constraints (6). To ensure the reliability of this analysis, data were routinely analyzed by two investigators independently.

1. Wülfing C, Purtic B, Klem J, Schatzle JD (2003) Stepwise cytoskeletal polarization as a series of checkpoints in innate but not adaptive cytolytic killing. *Proc Natl Acad Sci USA* 100:7767–7772.
2. Orange JS, et al. (2003) The mature activating natural killer cell immunologic synapse is formed in distinct stages. *Proc Natl Acad Sci USA* 100:14151–14156.
3. Orange JS (2008) Formation and function of the lytic NK-cell immunological synapse. *Nat Rev Immunol* 8:713–725.
4. Michaelson D, et al. (2001) Differential localization of Rho GTPases in live cells: regulation by hypervariable regions and RhoGDI binding. *J Cell Biol* 152:111–126.
5. Tskvitaria-Fuller I, et al. (2006) Specific patterns of Cdc42 activity are related to distinct elements of T cell polarization. *J Immunol* 177:1708–1720.
6. Singleton KL, et al. (2009) Spatiotemporal patterning during T cell activation is highly diverse. *Sci Signal* 2:ra15.
7. Billadeau DD, et al. (1998) The Vav-Rac1 pathway in cytotoxic lymphocytes regulates the generation of cell-mediated killing. *J Exp Med* 188:549–559.

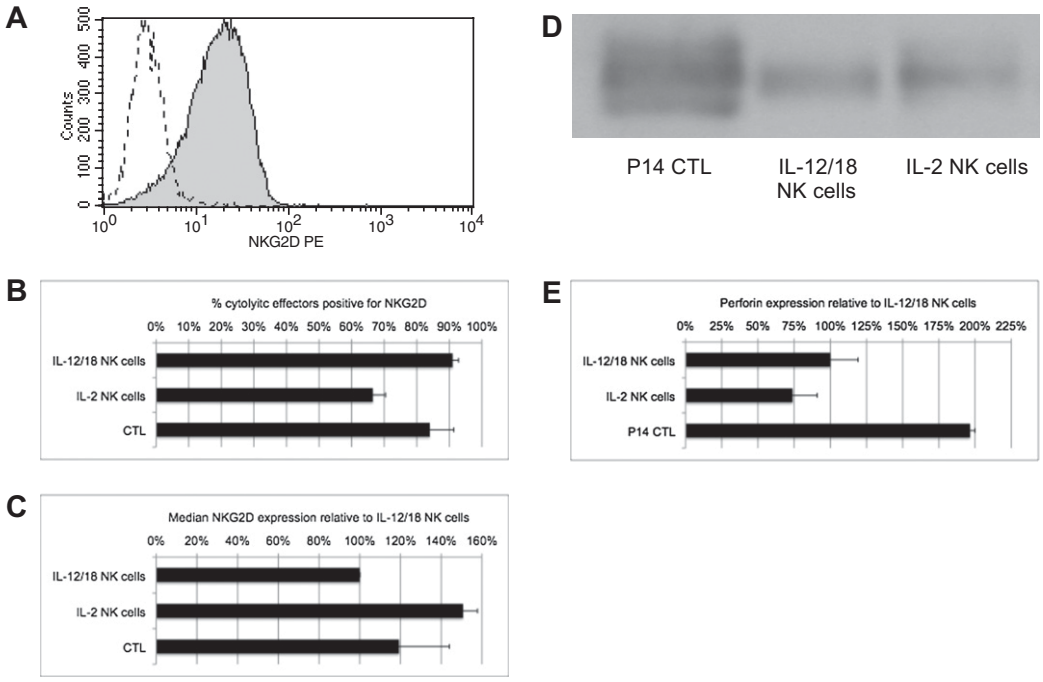

Fig. S1. Cytolytic effectors express comparable amounts of NKG2D and perforin (*A*–*C*) IL-12/18 NK cells, IL-2 NK cells, and CTL were analyzed for NKG2D expression by FACS in three to four independent experiments each. (*A*) A representative α-NKG2D stain of IL-12/18 NK cells. (*B*) The percentage of cytolytic effectors, as indicated, that is positive for NKG2D expression is given with SEs. (*C*) The median expression level of NKG2D-positive cytolytic effectors relative to expression in IL-12/18 NK cells is given with SEs. (*D* and *E*) The same cytolytic effectors were analyzed for perforin expression by Western blotting in three independent experiments. (*D*) A representative blot is given. (*E*) Integrated perforin band intensity was measured relative to that of GAPDH and such intensity is given with SEs normalized to that of IL-12/18 NK cells.

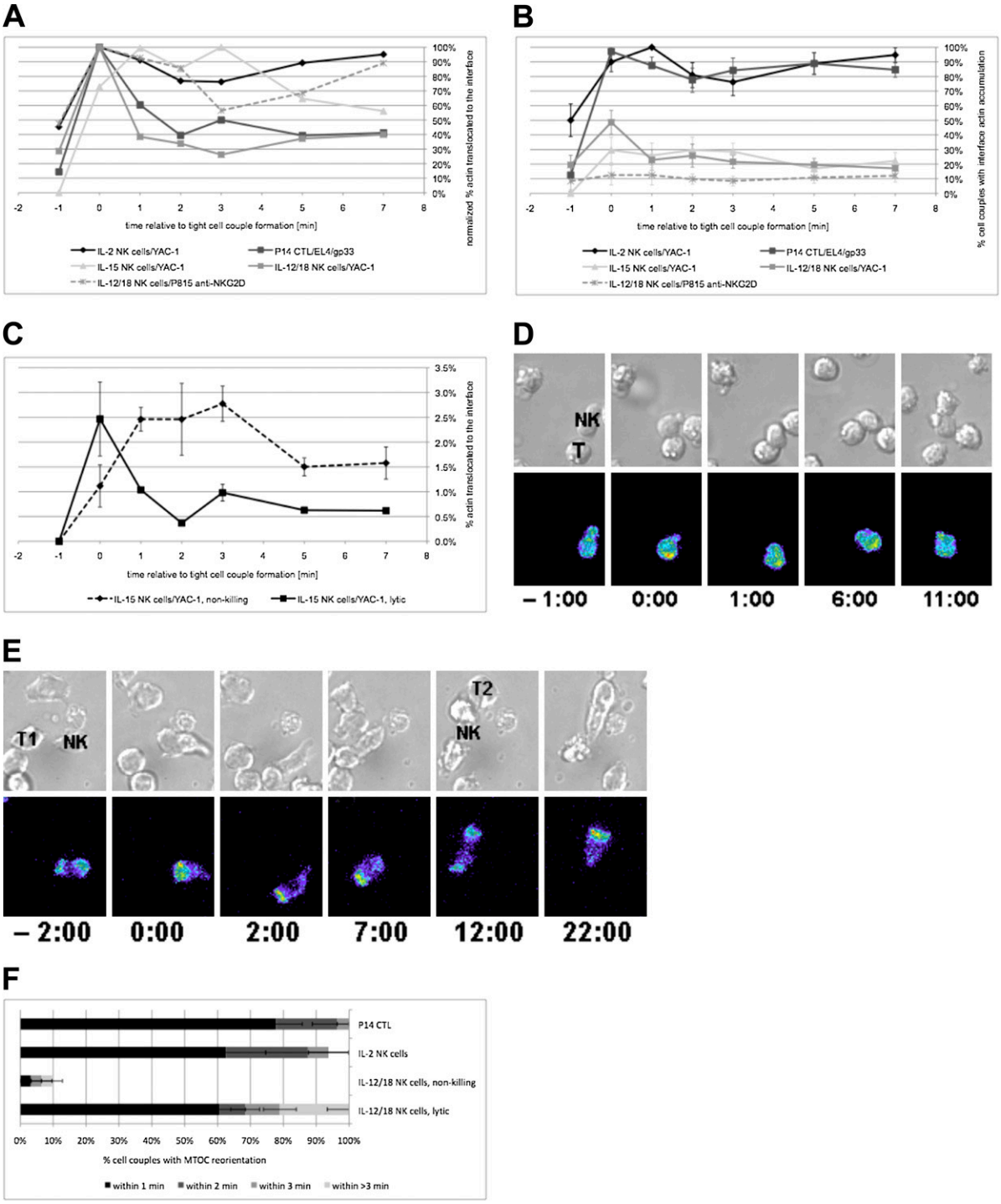

Fig. S2. Features of the polarization of cytolytic effectors (Fig. 1) (*A*) The percentage of actin-GFP translocated to the interface is given as a function of time relative to tight cell coupling as in Fig. 1*A* but normalized to the time point with most intense accumulation to allow easier comparison of its dynamics between cytolytic effectors. (*B*) The percentage of cell couples with interface Actin-GFP accumulation, a component in the calculation of the percentage of actin-GFP translocated to the interface, is given with SEs as a function of time relative to tight cell couple formation as in Fig. 1*A*. (*C*) For IL-15 NK cell/YAC-1 interactions, the data from Fig. 1*A* are displayed separately for nonkilling (broken line) and lytic (solid line) interactions. (*D* and *E*) Representative interactions of actin-GFP–transduced IL-15 (*D*) and IL-2 (*E*) NK cells with YAC-1 target cells (T) are shown at the indicated time points (in min) relative to the time of tight cell couple formation. The IL-2 NK cell interacts with two targets sequentially killing both. The IL-15 NK cell/target cell interaction is also lytic. Differential interference contrast images are shown in the top rows, with top-down, maximum projections of 3D actin-GFP fluorescence data in the bottom rows. The actin-GFP fluorescence intensity is displayed in a rainbow-like false-color scale (increasing from blue to red). Corresponding movies are Movie S4 and Movie S1, respectively. Movie S2 contains an alternate IL-2 NK cell. (*F*) The time between interface formation and the arrival of the MTOC at the center of the interface is given for the interactions of P14 T cells with EL4 target cells incubated with 10 μM gp33 agonist peptide, and IL-2 or IL-12/18 NK cells with YAC-1 target cells, as indicated. IL-12/18 NK cells were analyzed separately for nonkilling and lytic interactions as indicated. Cytolytic effectors were transduced with tubulin-GFP. On average 31 cell couples (range, 16–42) were analyzed per condition. Movie S8 contains representative IL-2 NK cell data. IL-12/18 NK cell and P14 CTL data were from Wülfing et al. (1).

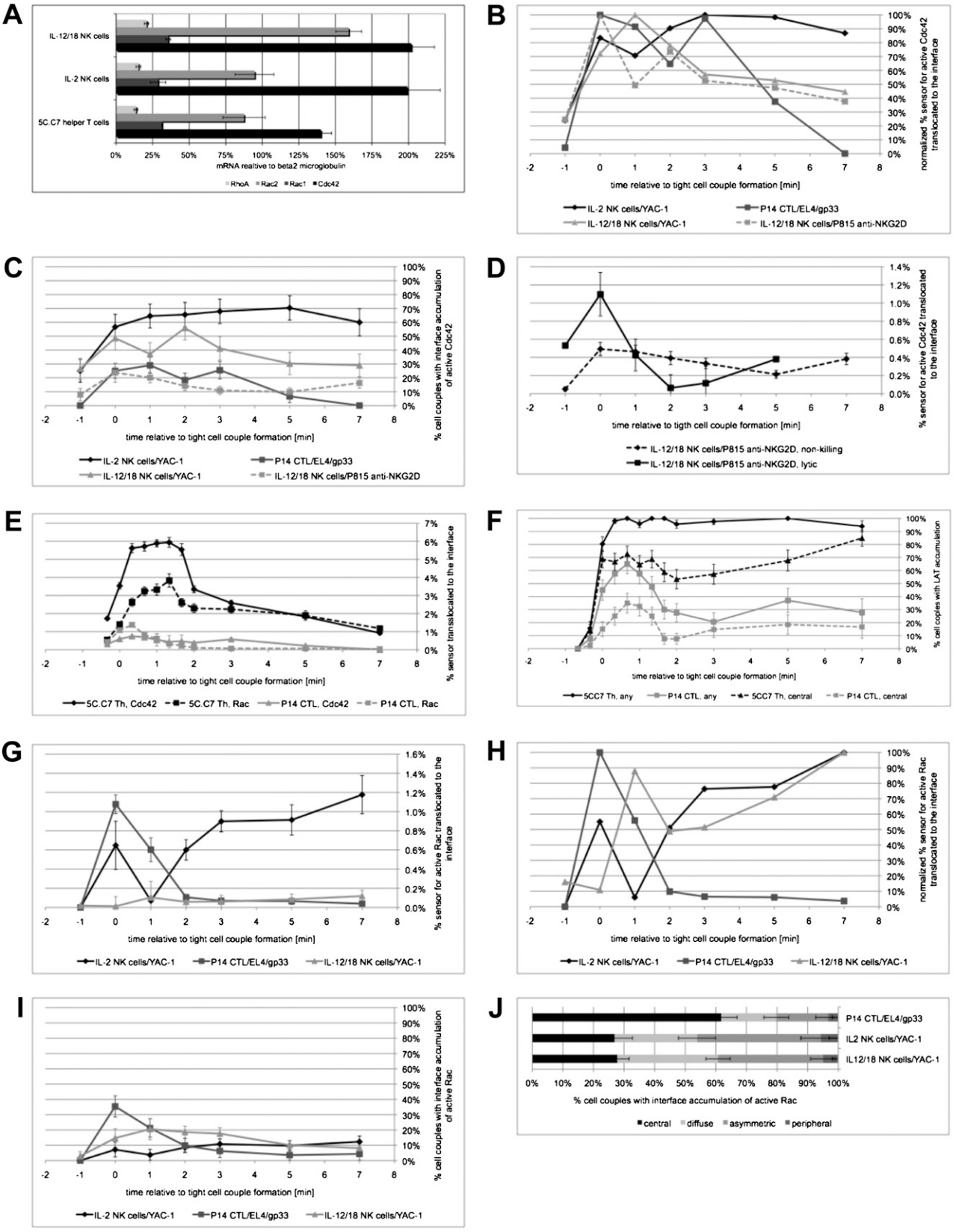

Fig. S3. Features of the interface accumulation of active Cdc42 and Rac (Fig. 3). (*A*) mRNA levels relative to those for β2-microglobulin as determined by real-time PCR from cDNA are given with SEs for the indicated mRNAs and the following cell types: IL-2 NK cells, IL-12/18 NK cells, and in vitro primed primary 5C.C7 T cells (6), as noted. Differences in mRNA levels between Cdc42 and Rac1 are significant ($P \leq 0.05$) for all cell types. Relative mRNA levels were determined two to six times per condition. (*B*) The percentage of sensor for active Cdc42 translocated to the interface is given as a function of time relative to tight cell coupling as

Legend continued on following page

in Fig. 3*A*, but normalized to the time point with most intense accumulation to allow easier comparison of its dynamics between cytolytic effectors. (*C*) The percentage of cell couples with interface accumulation of the sensor for active Cdc42, a component in the calculation of the percentage of sensor for active Cdc42 translocated to the interface, is given with SEs as a function of time relative to tight cell couple formation as in Fig. 3*A*. (*D*) For IL-12/18 NK cell/P815 α-NKG2D interactions, the data from Fig. 3*A* are displayed separately for nonkilling (broken line) and lytic (solid line) interactions. For lytic interactions, the number of cell couples analyzable at 7 min after tight cell coupling decreased to less than 10. This time point is therefore omitted. (*E*) The percentage of accumulation of sensors for active Cdc42 or Rac as indicated at the interface of P14 CTLs and EL4 target cells in the presence of 10 μM gp33 agonist peptide and at the interface of 5C.C7 T cells and CH27 B cell lymphoma APCs in the presence of 10 μM MCC agonist peptide (6) as noted is given with SEs as a function of time relative to tight cell couple formation. T cells were transduced with the sensors for active Cdc42 and Rac. Differences between P14 and 5C.C7 T cells are significant ($P < 0.01$) at all time points at or greater than 0 s for both the Cdc42 and Rac sensor. On average 28 cell couples (range, 20–47) were analyzed per condition. (*F*) The percentage of cell couples with interface LAT accumulation in any (solid line) or a central pattern (broken line) (6) as a function of time relative to tight cell couple formation is given with SEs for the interaction of P14 CTLs with EL4 target cells in the presence of 10 μM pg33 agonist peptide (gray) and 5C.C7 T cells with CH27 B cell lymphoma APCs in the presence of 10 μM MCC peptide (black) (6). T cells were retrovirally transduced with LAT-GFP. Differences in accumulation in any pattern are significant at $P \leq 0.001$ at all time points at or greater than 0 s. Forty and 51 cell couples were analyzed, respectively. (*G*) The percentage of sensor for active Rac translocated to the cytolytic effector/target cell interface is given as a function of time relative to tight cell coupling with SEs for the following interactions: P14 T cells/EL4 target cells/10 μM gp33 agonist peptide and IL-2 or IL-12/18 NK cells with YAC-1 target cells, as indicated. To account for low numbers of cell couples with interface Rac accumulation in IL-2 and IL-12/18 NK cells, time points 2 through 7 were averages of time points 1, 2, 3 to 6, 7, and 8, respectively. For CTLs, differences in the accumulation index relative to time 0 are significant at $P < 0.001$ at time points at or greater than 2 min. On average 37 cell couples (range, 24–48) were analyzed per condition. For normalized data and percentage of cell couples with accumulation displayed separately, see *H* and *I*. (*H*) The percentage of sensor for active Rac translocated to the interface is given as a function of time relative to tight cell coupling as in *G* but normalized to the time point with most intense accumulation to allow easier comparison of its dynamics between cytolytic effectors. (*I*) The percentage of cell couples with interface accumulation of the sensor for active Rac, a component in the calculation of the percentage of sensor for active Rac translocated to the interface, is given with SEs as a function of time relative to tight cell couple formation as in *G*. (*J*) Of all time points with interface accumulation from all cell couples analyzed for each condition, percent time points with interface accumulation of active Rac in the indicated pattern is given with SEs for the interactions defined in *G*. Differences in percentage of central accumulation of active Rac between CTLs and both NK cell types are significant at $P < 0.001$. On average, 95 time points (range, 57–140) from an average of 40 cell couples (range, 28–48) were analyzed.

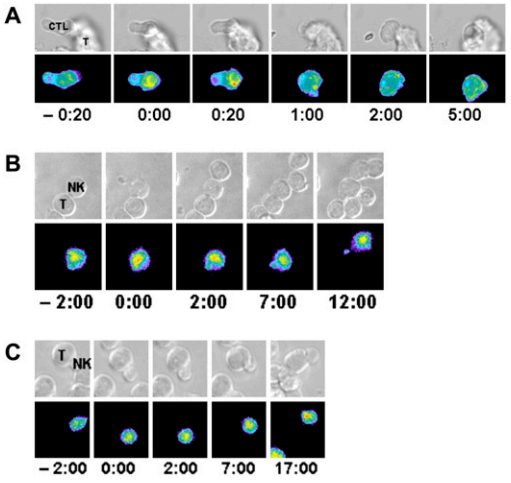

Fig. S4. Accumulation of active Rac at the cytolytic effector/target cell interface is weak and transient Similar to Fig. 2, representative interactions between cytolytic effectors (CTL or NK) transduced with a sensor for active Rac and their target cells (T) are shown as follows: (*A*) P14 CTL/Rac with EL4 target cell/10 μM gp33 agonist peptide (Movie S13); (*B*) IL-12/18 NK cell/Rac with YAC-1 target cell, nonkilling interaction (Movie S14; Movie S7 with alternate cell couple); and (*C*) IL-2 NK cell/Rac with YAC-1 target cell, nonkilling interaction (Movie S15).

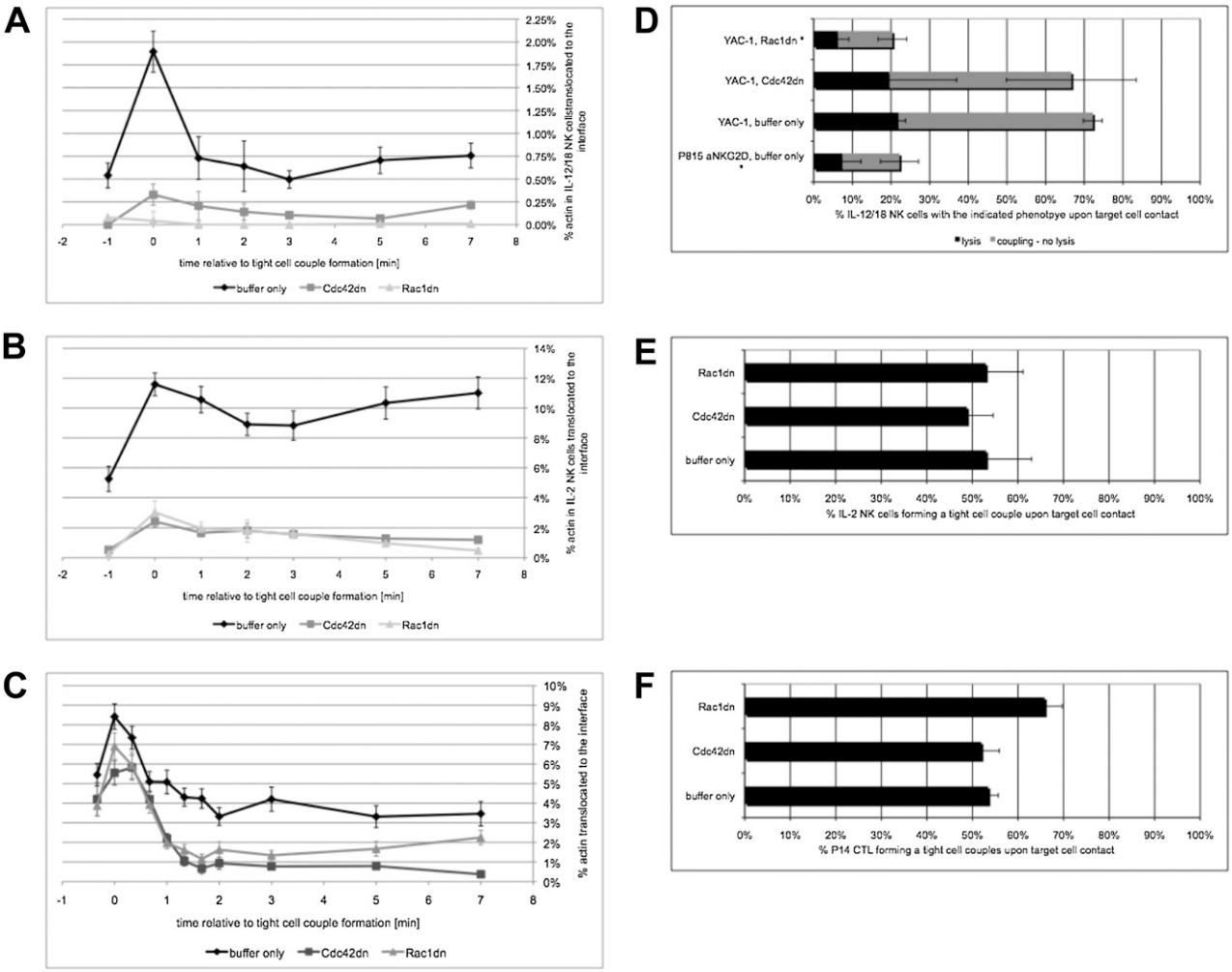

Fig. S5. Cdc42 and Rac regulate interface actin accumulation and cell coupling (*A*). The percentage of actin-GFP translocated to the interface of IL-12/18 NK cells transduced with actin-GFP and YAC-1 target cells in the presence of buffer only or 100 nM Cdc42dn/Rac1dn as protein transduction reagents as indicated is given with SEs as a function of time relative to tight cell couple formation. To account for low numbers of cell couples with interface actin accumulation, time points 3 through 7 were averages of time points 2, 3, 4 to 6, 7, and 8, respectively. Differences between buffer only and Cdc42dn are significant ($P < 0.005$) at all time points. Differences between buffer only and Rac1dn are significant ($P < 0.001$) at all time points. On average 30 cell couples (range, 18–37) were analyzed per condition. (*B*) The percentage of actin-GFP translocated to the interface of IL-2 NK cells transduced with actin-GFP and YAC-1 target cells in the presence of buffer only or 100 nM Cdc42dn/Rac1dn as protein transduction reagents as indicated is given with SEs as a function of time relative to tight cell couple formation. To account for low numbers of cell couples with interface actin accumulation in the treatment with Cdc42dn/Rac1dn, time points 3 through 7 were averages of time points 2, 3, 4 to 6, 7, and 8, respectively. Differences between buffer only and Cdc42dn and Rac1dn are significant ($P < 0.001$) at all time points. On average, 21 cell couples (range, 16–27) were analyzed per condition. (*C*) The percentage of actin-GFP translocated to the interface of P14 CTLs transduced with actin-GFP and EL4 target cells in the presence of 10 μM gp33 agonist peptide and buffer only or 100 nM Cdc42dn/Rac1dn as protein transduction reagents as indicated is given with SEs as a function of time relative to tight cell couple formation. Differences between buffer only and Cdc42dn are significant ($P < 0.001$) at all time points at or greater than 1 min. Differences between buffer only and Rac1dn are significant ($P < 0.01$) at time points 1 to 3 min. Differences between Cdc42dn and Rac1dn are significant ($P < 0.01$) at time point 7 min. On average 23 cell couples (range, 22–23) were analyzed per condition. (*D–F*) For the interactions of (*D*) IL-12/18 NK cells with YAC-1 target cells or P815 target cells incubated with α-NKG2D, (*E*) IL-2 NK cells with YAC-1 target cells, and (*F*) P14 CTLs with EL4 target cells in the presence of 10 μM gp33 agonist peptide, the percentage of cytolytic effectors that form a tight cell couple upon target cell contact is given with SEs upon addition of buffer only or 100 nM Cdc42dn/Rac1dn as protein transduction reagents. For IL-12/18 NK cells, the percentage of tight cell couples is further differentiated into lytic and nonkilling interactions. Asterisk indicates significance versus buffer only in the percentage of tight cell couple formation at $P < 0.001$. On average 109 cytolytic effectors (range, 52–349) were analyzed per condition.

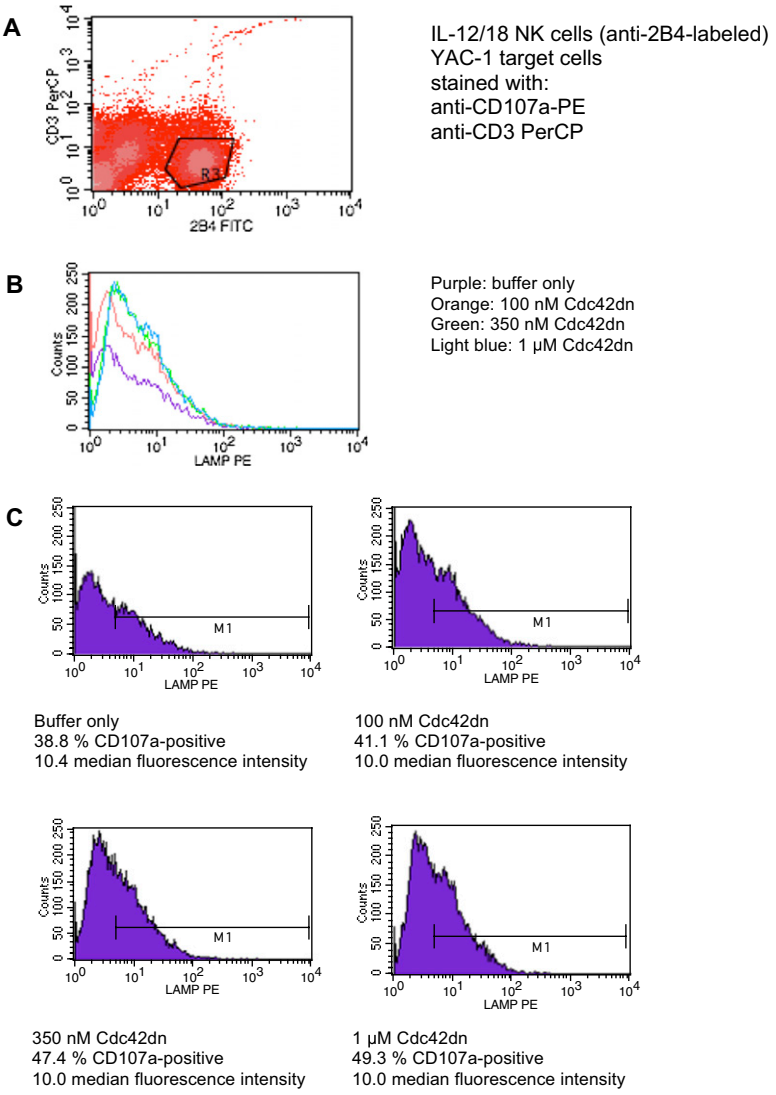

Fig. S6. (Continued)

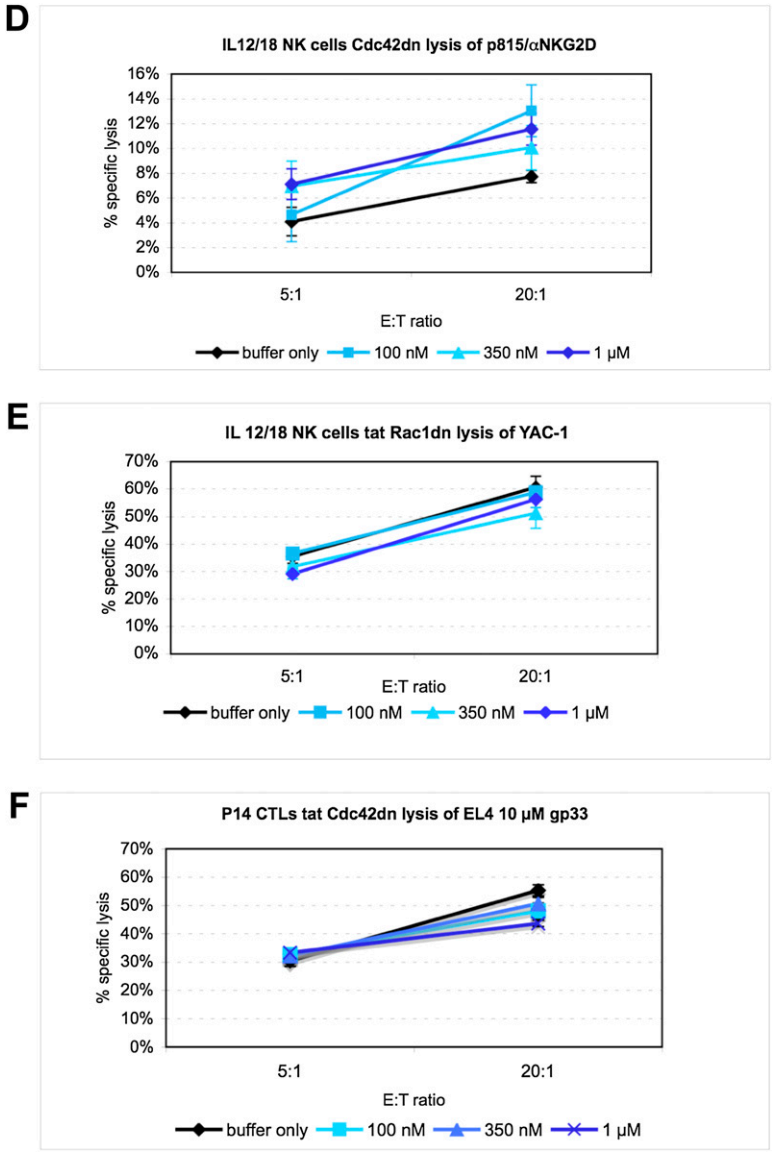

Fig. S6. Representative CD107a expression and chromium release assays (Fig. 4). (*A*–*C*) One representative CD107a (LAMP) expression assay is given for the interaction of IL-12/18 NK cells treated with Cdc42dn (buffer only to 1 μM) and YAC-1 target cells. (*A*) IL-12/18 NK cells were identified as being negative for CD3 and positive for CD244 (2B4) as shown for the buffer-only data. IL-12/18 NK cell/target cell couples had been dissociated before staining. (*B*) An overlay of CD107a-PE staining data for gated IL-12/18 NK cells treated with buffer only, 100 nM, 350 nM, or 1 μM Cdc42dn as indicated is given. (*C*) The same data as shown in *B* is displayed as individual panels with percentage of IL-12/18 NK cells that are positive for CD107a (M1 gate) and median fluorescence intensity of that population indicated. (*D*–*F*) Three representative chromium release killing assays are given. The cytolytic effector, target cell, and protein transduction reagent used are given in the title of each graph. Percent specific lysis with SEs is plotted as a function of the effector to target cell (E:T) ratio for different concentrations of the protein transduction reagent, as indicated.

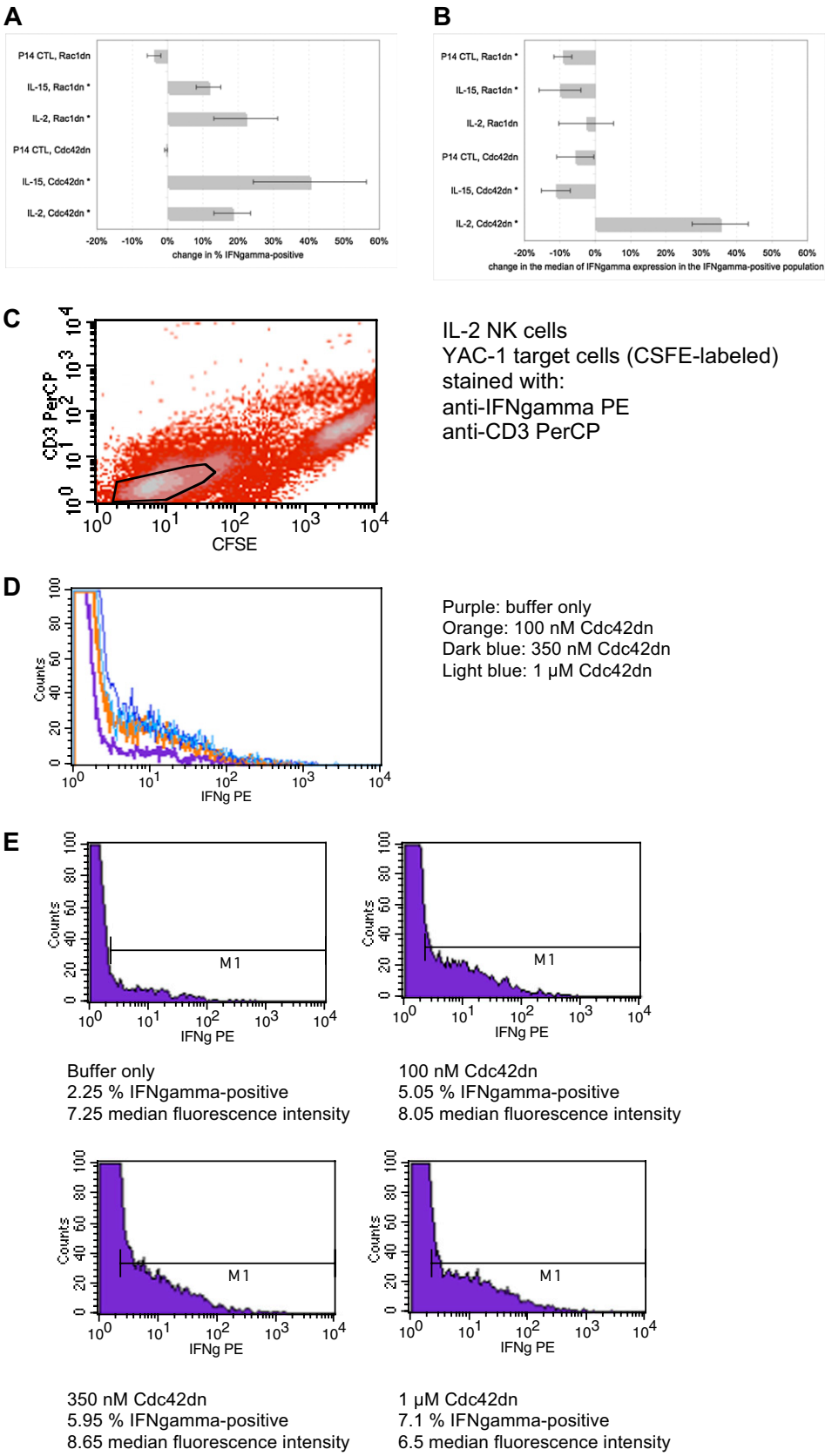

Fig. S7. Cdc42 and Rac regulate IFN-γ production. Changes in IFN-γ secretion upon treatment with 100 and 350 nM Cdc42dn or Rac1dn in the following interactions as indicated was analyzed: P14 T cells/EL4 target cells/10 μM gp33 agonist peptide and IL-2 or IL-15 NK cells/YAC-1 target cells. Percentage change upon treatment with Cdc42dn/Rac1dn in percent cytolytic effectors expressing IFN-γ (*A*) and in the median IFN-γ expression within this population (*B*) are displayed similar to Fig. 4 *B* and *C*. Three to four independent replicates of each assay were performed. (*C*–*E*) One representative IFN-γ production assay is given

Legend continued on following page

for the interaction of IL-2 NK cells treated with Cdc42dn (buffer only to 1 μM) and YAC-1 target cells. (*C*) IL-2 NK cells were identified as being negative for CD3 and carboxyfluorescein succinimidyl ester (used to label the YAC-1 target cells) as shown for the buffer only data. IL-2 NK cell/target cell couples had been dissociated before staining. (*D*) An overlay of IFN-γ–PE staining data for gated IL-2 NK cells treated with buffer only, 100 nM, 350 nM, or 1 μM Cdc42dn as indicated is given. (*E*) The same data as shown in *B* is displayed as individual panels with percentage of IL-2 NK cells that are positive for IFN-γ (M1 gate) and median fluorescence intensity of that population indicated. Raw analysis data are given in Table S2.

Table S1. Transient polarization of cytolytic effectors is related to efficient effector function

Table S1

Table S2. dc42 and Rac differentially regulate target cell lysis and IFN-γ secretion (Fig. 4 and Figs. S6 and S7)

Table S2

Analysis data from all bulk chromium release killing assays are given in the first third of the table. The top left cell of each table denotes the effector/target cell combination, the first column the concentration of protein transduction reagent. Percent specific lysis from individual assays are given with SEs in the second and fourth column for effector to target cell ratios of 20:1 and 5:1, respectively. In killing assays with moderately sensitive target cells, target cell lysis at the 5:1 effector-to-target cell ratio was too low for meaningful analysis. For killing of EL4 target cells by P14 CTLs in the presence of 1 nM gp33, killing levels varied substantially from assay to assay, likely because of the borderline strength of the stimulus. The corresponding average percentage change in specific lysis upon addition of the protein transduction reagent is given in the third and fifth column for effector to target cell ratios of 20:1 and 5:1, respectively. Pooled data for addition of 100 and 350 nM protein transduction reagent derived from the second and third column are displayed in Fig. 4*D*. Representative killing assays are given in Fig. S6 *D-F*.

Analysis data from all CD107a (LAMP) expression assays are given in the second third of the table. The top left cell of each table denotes the effector/target cell combination, the first column the concentration of protein transduction reagent. Percent NK cells expressing CD107a and average percentage change thereof upon addition of the protein transduction reagent are given in the second and third column. Median fluorescence intensity of the CD107a-positive NK cells and average percent change thereof upon addition of the protein transduction reagent are given in the fourth and fifth column. These data were not available for IL-15 NK cells. Pooled data for addition of 100 nM and 350 nM protein transduction reagent derived from the second and third column are displayed in Fig. 4*B*. Pooled data for addition of 100 and 350 nM protein transduction reagent derived from the fourth and fifth column are displayed in Fig. 4C. A representative CD107a expression assay is given in Fig. S6 *A-C*.

Analysis data from all IFN-γ production assays are given in the last third of the table. The top left cell of each table denotes the effector/target cell combination, the first column the concentration of protein transduction reagent. Percent cytolytic effectors with intracellular IFN-γ and average percent change thereof upon addition of the protein transduction reagent are given in the second and third column. Median fluorescence intensity of the IFN-γ-positive cytolytic effectors and average percent change thereof upon addition of the protein transduction reagent are given in the fourth and fifth column. Pooled data for addition of 100 nM and 350 nM protein transduction reagent derived from the second and third column are displayed in Fig. S7*A*. Pooled data for addition of 100 nM and 350 nM protein transduction reagent derived from the fourth and fifth column are displayed in Fig. S7*B*. A representative IFN-γ production assays is given in Fig. S7 *C-E*.

SI Movies 1–15.

Movie (related)	Fig.	Time between frames–expt.	Frames per second–movie	Cytolytic effector–target	Sensor	Cell coupling (frame/time)	Features
S1 (S2)	S2E	1 min	2	IL-2 NK–YAC-1	Actin-GFP	5/2 min (bottom) 16/7 min (top)	Blebbing, slow disintegration of the bottom target
S2 (S1)	–	1 min	2	IL-2 NK–YAC-1	Actin-GFP	3/1 min	Blebbing, slow disintegration of the target
S3 (S11)	2B	1 min	2	IL-2 NK–YAC-1	Sensor for active Cdc42	10/4 min (top) 19/9 min (bottom)	Blebbing and disintegration of both targets
S4	S2D	1 min	2	IL-15 NK–YAC-1	Actin-GFP	2/0 min	17/ 8 s: membrane rupture of the target
S5	–	10 s	6	IL-15 NK–YAC-1	–	3 min, 40 min	Membrane rupture of the central target
S6 (S9, S10)	–	1 min	2	IL-12/18 NK–YAC-1	Sensor for active Cdc42	5/2 min	19/ 9 s: Target cell disintegration
S7 (S14)	–	1 min	2	IL-12/18 NK–YAC-1	Sensor for active Rac	2/0 min	6/2 s: Membrane rupture
S8	–	1 min	2	IL-2 NK–YAC-1	Tubulin-GFP	5/2 min	Nonkilling interaction
S9 (S6, S10)	2A	1 min	2	IL-12/18 NK–YAC-1	Sensor for active Cdc42	6/2 min	Nonkilling interaction
S10 (S6, S9)	–	1 min	2	IL-12/18 NK–YAC-1	Sensor for active Cdc42	2/0 min	Nonkilling interaction (higher resolution)
S11 (S3)	–	1 min	2	IL-2 NK–YAC-1	Sensor for active Cdc42	6/2 min	Nonkilling interaction (higher resolution)
S12	2C	20 s	2	P14 CTL–EL4 10 μM gp33	Sensor for active Cdc42	9/ 4 min	Nonkilling interaction
S13	S4A	20 s	2	P14 CTL–EL4 10 μM gp33	Sensor for active Rac	8/3 min	–
S14 (S7)	S4B	1 min	2	IL-12/18 NK–YAC-1	Sensor for active Rac	4/1 min	Nonkilling interaction
S15	S4C	1 min	2	IL-2 NK–YAC-1	Sensor for active Rac	4/1 min	Nonkilling interaction

Representative interactionsof sensor-transduced cytolytic effectors with target cells are shown. DIC images are shown on top, with matching top-down, maximum projections of 3-dimensional sensor fluorescence data on the bottom. The sensor fluorescence intensity is displayed in a rainbow-like false-color scale (increasing from blue to red). Movie S5 only contains DIC images. The table lists for each movie other movies using the same experimental conditions ("related"), the corresponding manuscript figure ("Fig"), time between subsequent acquisitions in the experiment ("Time between frames – expt".), frame rate of the movie, the cytolytic effector and its target, the sensor expressed by the cytolytic effector ("Sensor"), the time of cytolytic effector – target cell couple formation given both as the movie frame number and the displayed movie time ("Cell coupling"), and noteworthy features of the movie. Some movies contain two sequential cytolytic effector – target cell interactions, as indicated by the positions of the respective targets relative to the effector.

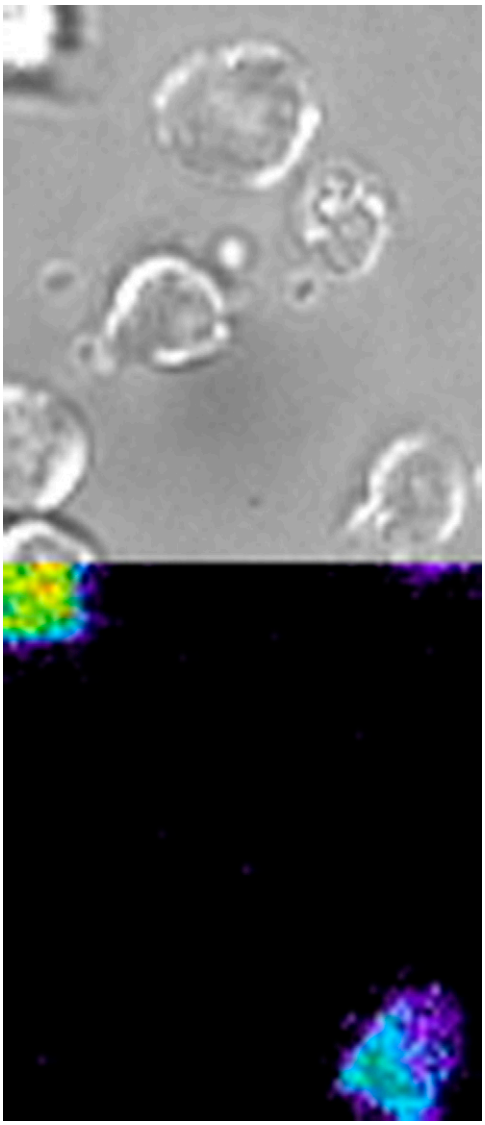

Movie S1

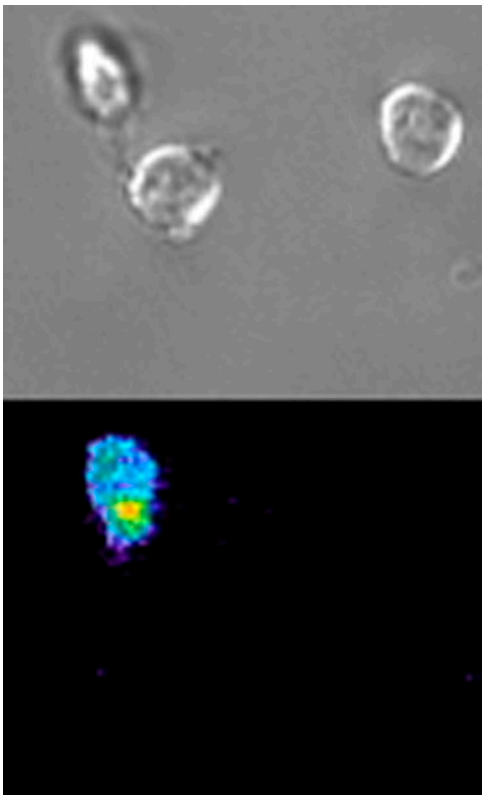

Movie S2

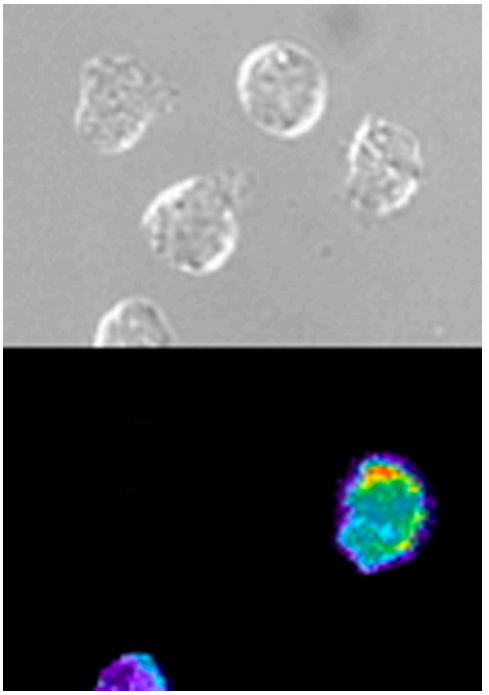

Movie S3

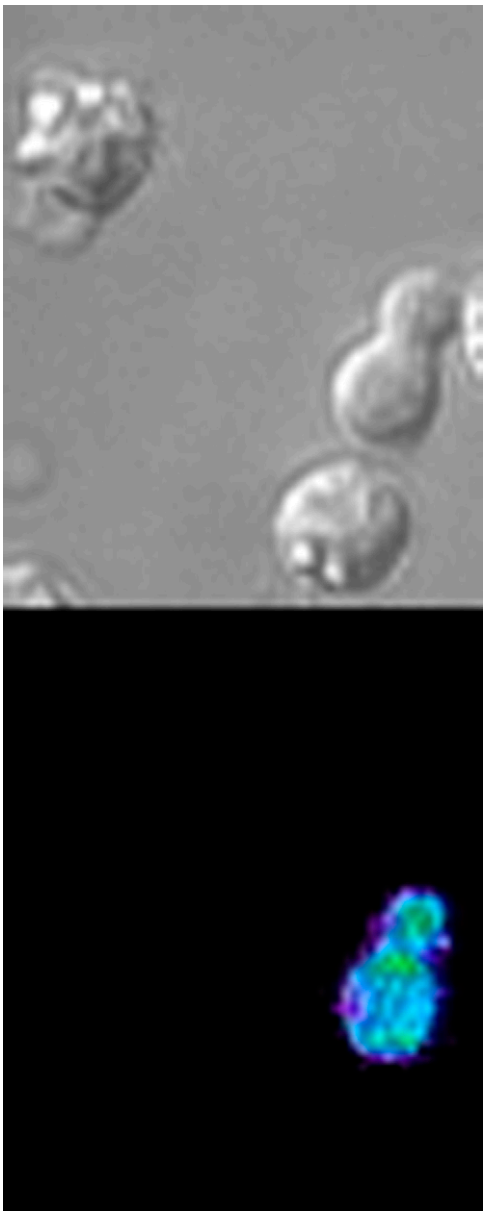

Movie S4

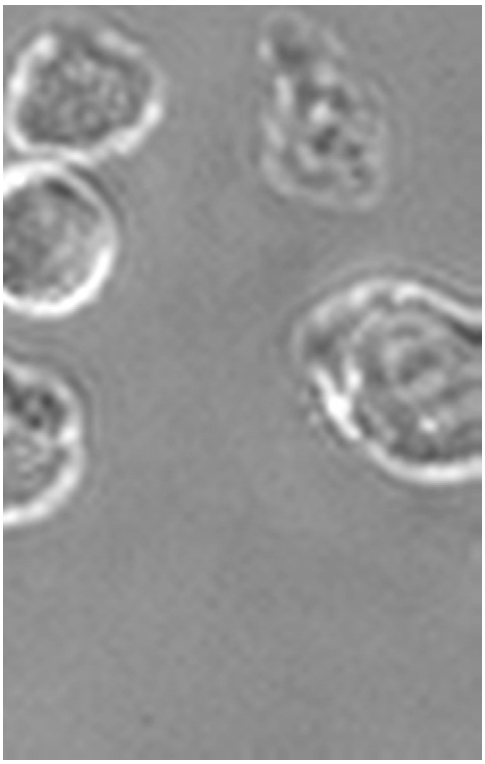

Movie S5

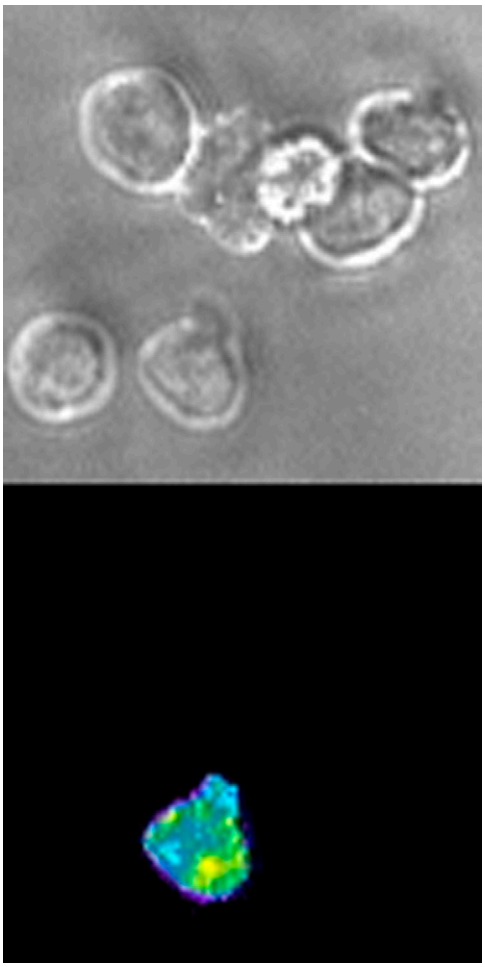

Movie S6

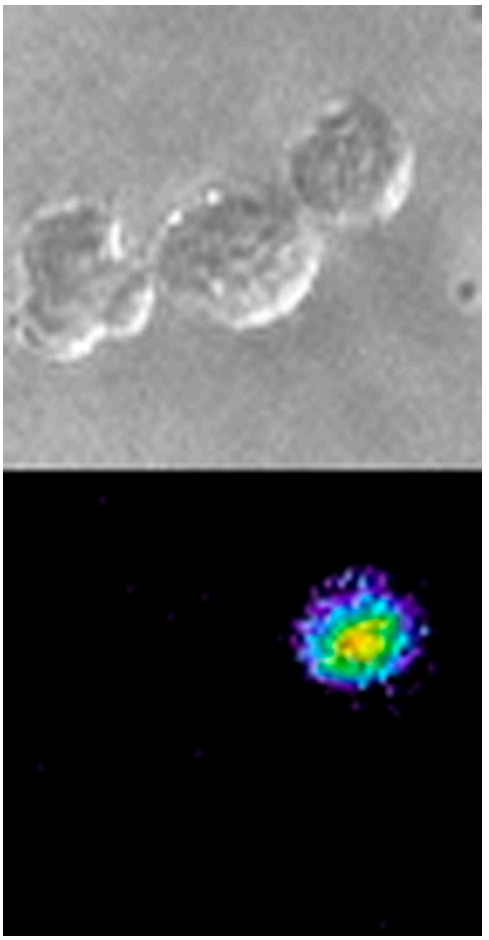

Movie S7

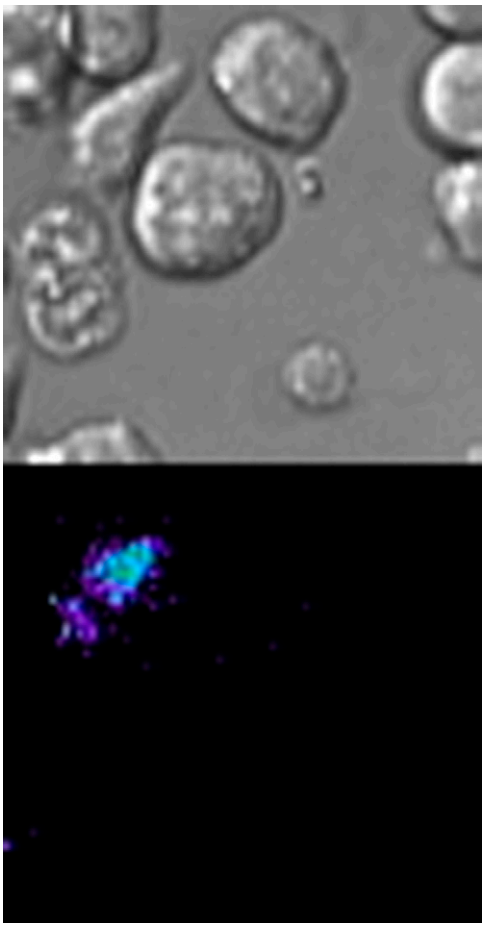

Movie S8

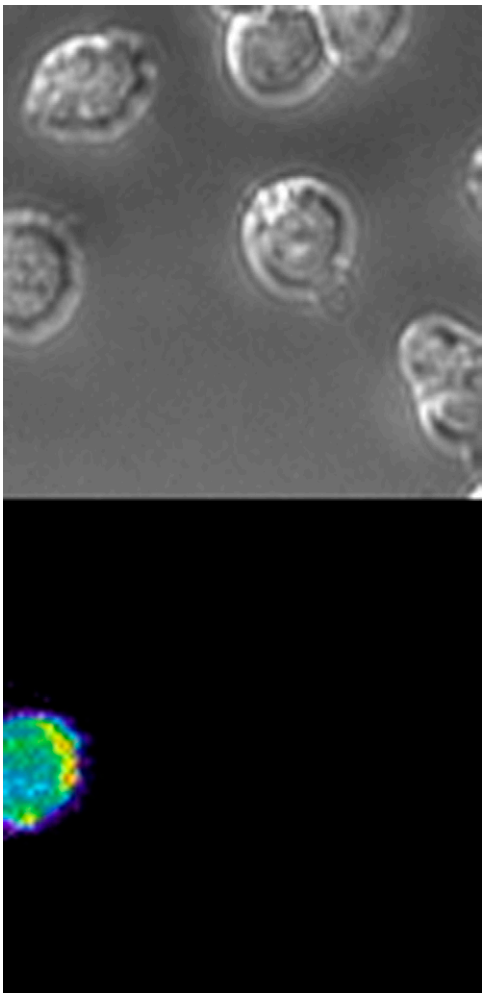

Movie S9

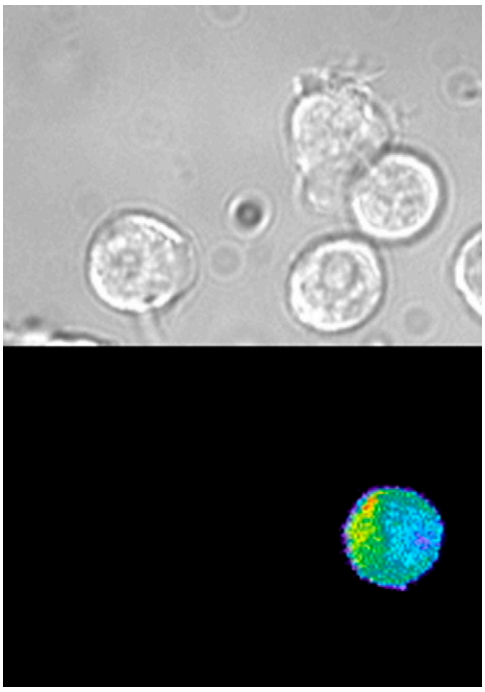

Movie S10

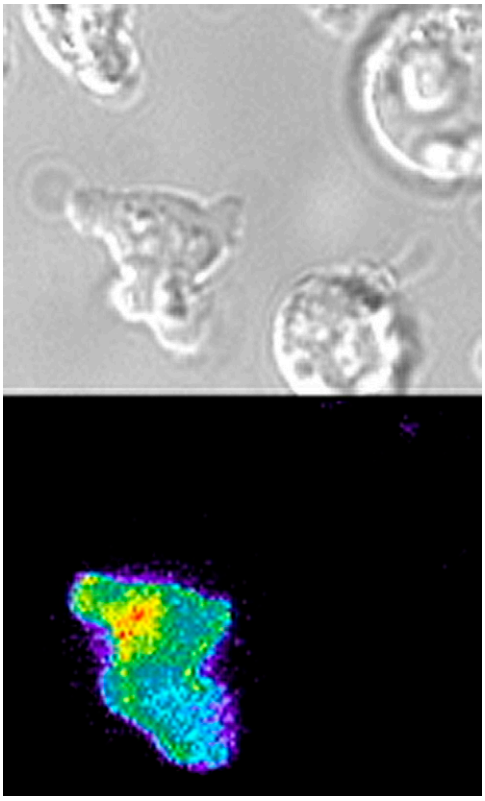

Movie S11

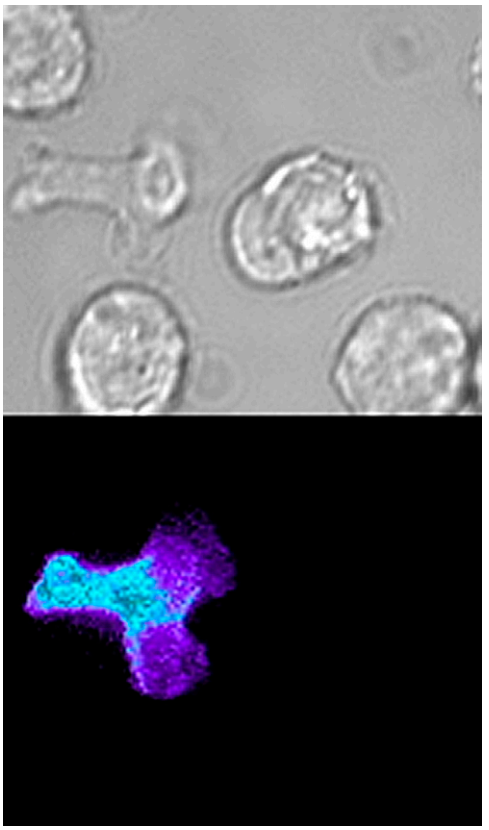

Movie S12

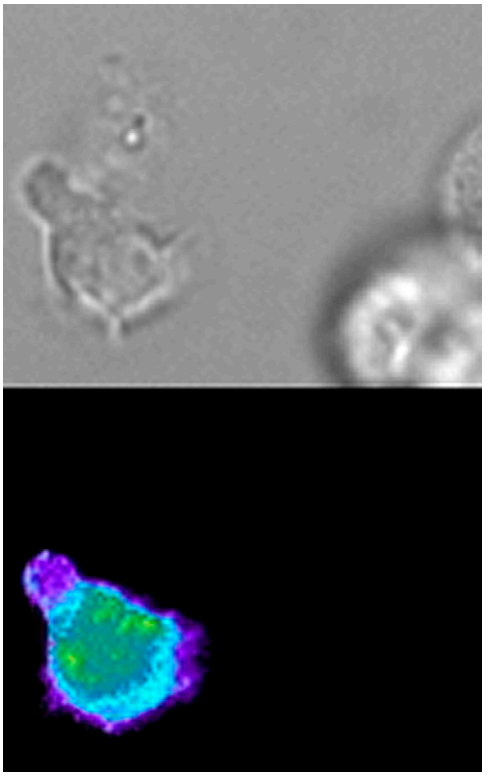

Movie S13

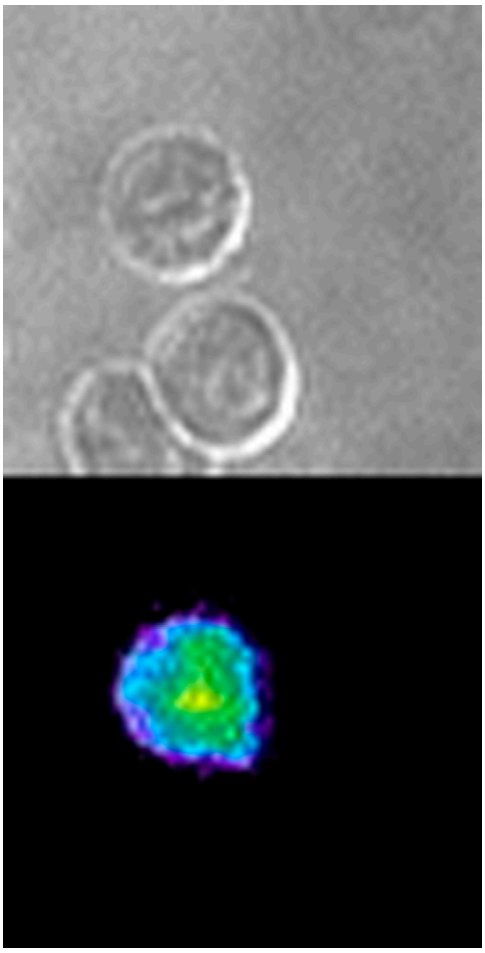

Movie S14

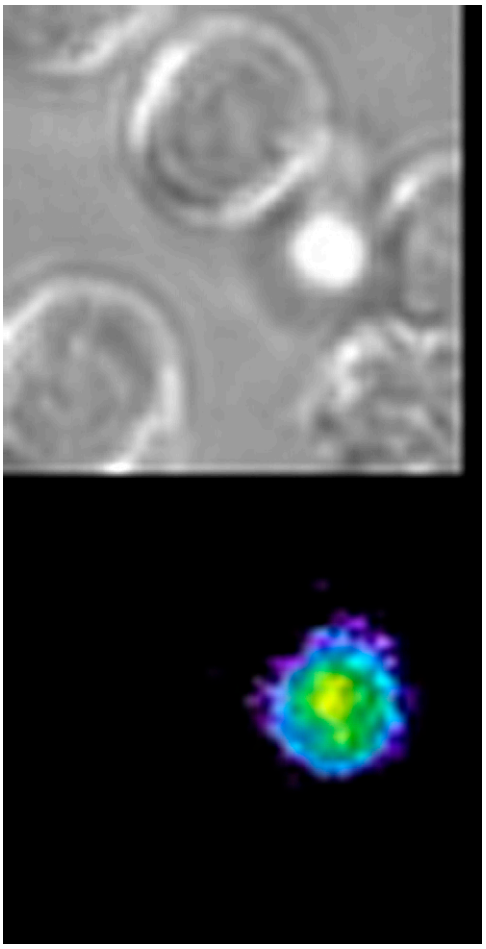

Movie S15